J Anim Reprod Biotechnol 2022;37:87-95
pISSN: 2671-4639 • eISSN: 2671-4663
https://doi.org/10.12750/JARB.37.2.87

JARB
Journal of Animal Reproduction and Biotechnology
Check for updates

Original Article

Testosterone secretion is affected by receptor tyrosine kinase c-Kit and anoctamin 1 activation in mouse Leydig cells

Eun-A Ko[1], Min Seok Woo[2] and Dawon Kang[2,3,*]

[1]Department of Physiology, Colledge of Medicine, Jeju National University, Jeju 63243, Korea
[2]Department of Physiology, College of Medicine and Institute of Health Sciences, Gyeongsang National University, Jinju 52727, Korea
[3]Department of Convergence Medical Science, Gyeongsang National University, Jinju 52727, Korea

Received May 12, 2022
Accepted May 22, 2022

***Correspondence**
Dawon Kang
E-mail: dawon@gnu.ac.kr

Author's Position and Orcid no.
Ko E-A, PhD professor,
https://orcid.org/0000-0002-1585-6886
Woo MS, PhD,
https://orcid.org/0000-0002-0357-9666
Kang D, PhD professor,
https://orcid.org/0000-0001-7402-7298

ABSTRACT Receptor tyrosine kinase c-Kit, a marker found on interstitial cells of Cajal (ICCs), is expressed in Leydig cells, which are testicular interstitial cells. The expression of other ICC markers has not yet been reported. In this study, we investigated the expression of c-Kit and anoctamin 1 (ANO1), another ICC marker, in mouse testes. In addition, the relationship between c-Kit and ANO1 expression and Leydig cell function was investigated. We observed that c-Kit and ANO1 were predominantly expressed in mouse Leydig cells. The mRNA and protein of c-Kit and ANO1 were expressed in TM3, a mouse Leydig cell line. LH induced an increase in intracellular Ca^{2+} concentration, membrane depolarization, and testosterone secretion, whereas these signals were inhibited in the presence of c-Kit and ANO1 inhibitors. These results show that c-Kit and ANO1 are expressed in Leydig cells and are involved in testosterone secretion. Our findings suggest that Leydig cells may act as ICCs in testosterone secretion.

Keywords: ANO1, c-Kit, Leydig cells, mice, testosterone

INTRODUCTION

Interstitial cells of Cajal (ICCs) are interstitial cells found in the gastrointestinal (GI) tract. They are well known to serve as pacemaker cells in the GI tract, which is characterized by the initiation of electrical slow waves and spontaneous rhythmic contractions (Popescu et al., 2006; Sanders, 2019). ICCs are electrically coupled by gap junction with adjacent smooth muscle cells, and propagate signals which produce smooth muscle contraction (Hennig et al., 2010; Parsons and Huizinga, 2020). Considering that ICCs act as pacemakers in the GI tract, there will be cells exhibiting ICC characteristics in other regions of the GI tract as well. ICC markers have been developed to detect these cells.

ICCs express c-Kit, encoding the receptor tyrosine kinase Kit, which was first known as an ICC marker and is now used widely (Gomez-Pinilla et al., 2009; Loera-Valencia et al., 2014). c-Kit has also been used as a marker to characterize hematopoietic, cardiac, and lung stem/progenitor cells (Edling and Hallberg, 2007; Liu et al., 2015). In addition to c-Kit, Ca^{2+}- dependent Cl- channel anoctamin 1 (ANO1, TMEM16A), has become known as an ICC marker. Therefore, ICCs can be recognized using antibodies to ANO1 and c-Kit alone or in combination (Chevalier et al., 2020; Drumm et al., 2020; Drumm et al.,

2021; Choi et al., 2022; Drumm et al., 2022). ANO1 has been reported to be a better marker than c-Kit for transcript analysis of single ICCs *in vitro* (Loera-Valencia et al., 2014). It has also been reported that c-Kit-negative ICCs are present in the subserosal layer of the mouse colon (Tamada and Kiyama, 2015).

Cells with immunological and morphological phenotypes similar to those of ICCs have been identified in the urinary tract, bladder, male genital organs, and the anterior vaginal wall in pelvic organ, suggesting that they act as pacemakers (Shafik et al., 2005; Wang et al., 2013; Sferra et al., 2019; Ma et al., 2020; Wishahi et al., 2021). Leydig cells are known as interstitial cells localized in the seminiferous tubules of testes, which play a major role in the production of androgens (Zirkin and Papadopoulos, 2018; Ishida et al., 2021; O'Donnell et al., 2022). Leydig cells play an important role in male reproduction, with functions such as steroidogenesis, androgen synthesis and secretion, and maintenance of spermatogenesis. c-Kit is expressed in Leydig cells and contributes to a steroidogenic function of Leydig cells *in vivo* (Rothschild et al., 2003). Reduced expression of c-Kit in Leydig cells is associated with increased apoptosis in subfertile human testes (Feng et al., 1999).

This study was performed to identify ANO1 expression in Leydig cells. In addition, changes in intracellular Ca^{2+} concentration ($[Ca^{2+}]_i$) and membrane potential were measured to determine whether Leydig cells might play a role similar to ICCs.

MATERIALS AND METHODS

Chemicals

Unless otherwise stated, culture media and other chemicals were purchased from Sigma Chemical Co. (St. Louis, MO, USA). The stock solution was made by dissolving luteinizing hormone (LH, 25 unit/mL), imatinib (10 mM), flufenamic acid (10 mM) in distilled water, dimethyl sulfoxide (DMSO), and ethanol, respectively. All compounds were diluted to their working concentration in the culture medium. When DMSO or ethanol was used as a solvent, control solution of the same concentration was used. The final concentration of DMSO or ethanol in working solution was diluted to ≤ 0.1%.

Animals and testis isolation

Male mice (C57BL/6J, six weeks old) were obtained from Central Lab. Animal Inc. (Seoul, Korea). The mice were kept in a pathogen-free environment for one week, with free access to food and water, and a 12-hour light-dark cycle. At seven weeks of age, testes were isolated from mice. Animal experiments were performed according to the guidelines of the Gyeongsang National University Animal Care and Use Committee (GNU-200702-M0041).

Hematoxylin and eosin (H&E) staining

Hematoxylin and eosin (H&E) solution was used to examine histological changes in testes. The H&E staining was performed as previously reported (Siregar et al., 2019). The tissues were fixed in 4% paraformaldehyde solution overnight at 4℃, washed in 0.1 M PBS, embedded in paraffin, and cut into 5 μm-thick slices. The paraffin slices were air-dried on gelatin-coated slides before being deparaffinized and washed with tap water. After being cleaned, the tissue sections were immerged in hematoxylin solution for 5 min. The degree of hematoxylin staining was examined in tap water, followed by 5 min of eosin staining. The sections were dehydrated in a series of alcohols (70% to 100% ethanol, 3 min each), then cleaned in xylene and mounted using permount mounting media (Fisher Chemical, Geel, Belgium). A BX61VS microscope (Olympus, Tokyo, Japan) was used to examine and photograph the stained tissue sections. Five portions of each sample were analyzed.

Immunohistochemistry (IHC)

Immunohistochemistry was used to determine the expression and localization of c-Kit and ANO1 in testis sections. The IHC was performed as previously reported (Siregar et al., 2019). Deparaffinized tissue slices were permeabilized for 10 min at room temperature with 0.2% Triton X-100. After three PBS washes, the sections were incubated for 60 min at room temperature in blocking buffer (10% normal goat serum in 0.1 M PBS). The sections were then incubated overnight at 4℃ with rabbit polyclonal anti-c-Kit and ANO1 primary antibodies (1:200 dilutions, Abcam, Cambridge, UK). The sections were incubated in the dark for 1.5 h after three washed in PBS with FITC-conjugated anti-rabbit IgG secondary antibody (Abcam) diluted at 1:400 in PBS. Finally, the sections were washed three times in PBS and stained for nuclei using

propidium iodide (PI). The stained sections were wet-mounted with Gel/Mount™ (Biomeda Corp., Foster City, CA, USA) and examined with a confocal laser scanning microscope (Olympus).

Cell culture

Mouse Leydig cell line TM3 (American Type Culture Collection, MD, USA) was generously provided by Dr. Jung Hye Shin (Namhae Garlic Research Institute, Namhae, Korea). Cell culture was performed as previously described (Yang et al., 2019). The cells were grown in Dulbecco's modified Eagle's medium (DMEM; Gibco/Life technologies, Grand Island, NY, USA) supplemented with 10% fetal bovine serum (FBS; Gibco), 100 U/mL penicillin (Gibco), and 100 mg/mL streptomycin (Gibco). The cells were incubated at 37℃ in a gas combination of 95% air and 5% CO_2, with the media changed every other day.

Isolation of total RNA and reverse transcriptase-polymerase chain reaction (RT-PCR)

TRIzol™ Reagent (Invitrigen, Carlsbad, CA, USA) was used to extract total RNA from TM3 cells according to the manufacturer's instructions. The total RNA isolation and RT-PCR were performed as previously described (Siregar et al., 2019). The TRIzol™ Reagent was added directly to the cells in the culture dish after washing them three times with 1 × PBS. The cells were scrapped and lysed by pipetting up and down several times. The cell homogenate was transferred to an Eppendorf tube and incubated at room temperature for 5 min to allow the nucleoprotein complex to completely dissociate. Chloroform was added to 20% of the TRIzol's volume and forcefully shaken for 15 sec. After 3 min incubation at room temperature, the mixture was centrifuged for 10 min at 12,000 × g at 4℃. The aqueous sample was transferred to a new Eppendorf tube, precipitated with 100% isopropanol, and kept at room temperature for 10 min before being centrifuged at 12,000 × g for 10 min at 4℃. The RNA pellets were washed in 75% ethanol, vortexed briefly, centrifuged at 7,500 × g for 5 min at 4℃, air-dried for 10 min, and re-suspended in RNase-free water treated with diethyl pyrocarbonate (DEPC).

A reverse transcriptase kit (DiaStartTM RT kit; SolGent, Daejeon, Korea) was used to synthesize the first-strand cDNA from the extracted total RNA (3 μg). PCR amplification was carried out with first-strand cDNA, Taq polymerase (G-Taq, Cosmo Genetech, Seoul, Korea), and specific primers for mouse *c-Kit* (#NM_001122733.1, forward: 5'-ATAGACCCGACGCAACTTCCT-3' and reverse: 5'- AACTGTCATGGCAGCATCCGAC-3'), ANO1 (#NM_178642.6, forward: 5'-CAACTACCGATGGGACCT-CAC-3' and 5'-AATAGG CTGGGAATCGGTCC-3'). Glyceraldehydes-3-phosphate dehydrogenase (GAPDH, #NM_017008, forward: 5'- CTA AAG GGC ATC CTG GGC -3' and reverse: 5'- TTA CTC CTT GGA GGC CAT -3') was used as a loading control. For PCR, initial denaturation at 94℃ for 5 min was followed by 35 cycles at 94℃ for 30 sec, 59℃ for 30 sec, and 72℃ for 30 sec, followed by a final extension step at 72℃ for 10 min. To confirm the product size, the PCR products were electrophoresed on a 1.5% (w/v) agarose gel. The iBright™ CL1500 imaging system (Thermo Scientific Fisher/Life Technologies Holdings Pte Ltd., Singapore) was used to captured and visualized images of DNA fragments. The ABI PRISM® 3100-Avant Genetic Analyzer (Applied Biosystems, CA, USA) was used to sequence the DNA fragments directly.

Western blot analysis

The Western blot analysis was performed as previously described (Yang et al., 2019). TM3 cells (5×10^4 cells/60-mm dish) were exposed to various testosterone concentrations for 24 h. RIPA buffer (Thermo Fisher Scientific., Waltham, MA, USA) containing 1 × protease inhibitor cocktail (Roche Diagnostics., Indianapolis, IN, USA) was used to separate total protein from TM3 cells. The cell lysates were cleared by centrifugation at 15,871 × g (13,000 rpm, Eppendorf, Hamburg, Germany) at 4℃ for 20 min after being incubated for 30 min on ice with intermittent vortexing. A Pierce bicinchoninic acid (BCA) protein assay kit (Thermo Fisher Scientific) was used to determine the protein concentration in cell lysates. Equal amounts of proteins mixed with 1 × loading buffer were electrophoresed for 2 h at 100 V on 8% sodium dodecyl sulfate (SDS)-polyacrylamide gel, and the gel was blotted onto a polyvinylidene difluoride (PVDF, Millipore, Billerica, MA, USA) membrane using a tank transfer method for 70 min at 100 V. Membranes were blocked with 5% (*w/v*) fat-free dry milk in tris buffered saline with Tween20 (TBST; 20 mM Tris HCl (pH 8), 150 mM NaCl, and 0.1% Tween-20) for 120 min at room temperature before being incubated with polyclonal anti-c-Kit and ANO1 antibodies (1:1,000 dilution, Abcam) or monoclonal anti-β-actin

antibody (1:5,000 dilution) at 4℃ overnight. At the end of the primary antibody incubation, a secondary horseradish peroxidase (HRP)-conjugated anti-rabbit or anti-mouse antibody at 1:10,000 (Assay Designs, Ann Arbor, MI, USA) was added. Immuno-positive bands were developed by an enhanced chemiluminescence (Thermo Fisher Scientific), and visualized with the iBright™ CL1500 imaging system (Thermo Scientific Fisher/Life Technologies Holdings Pte Ltd.). The relative protein level was determined with β-actin used as a loading control.

Measurement of intracellular Ca^{2+} concentration

As previously stated (Yang et al., 2019), intracellular Ca^{2+} concentration was measured using a confocal laser scanning microscope equipped with a fluorescence system (IX70 Fluoview, Olympus). TM3 cells cultured on a glass-bottom culture dish (SPL) were incubated with 5 μM Fluo-3AM in serum free DMEM media for 30 min before being washed three times with 1 × PBS. Each fluorescent image was scanned every 5 sec at 488 nm on an excitation argon laser and 530 nm long pass emission filters. At the single-cell level, all scanned images were processed to analyze changes in intracellular Ca^{2+} concentration $[Ca^{2+}]_i$. To account for variations in basal fluorescence intensity, the changes in $[Ca^{2+}]_i$ were computed as fluorescence intensity (F) divided by the basal fluorescence intensity before treatment (F_0). The changes in $[Ca^{2+}]_i$ were recorded for 8 min following treatment with chemicals, because the change in $[Ca^{2+}]_i$ is an immediate reaction in response to chemicals.

Measurement of plasma membrane potentials

As described previously (Yang et al., 2019), the plasma membrane potential was measured using the FluoVolt™ membrane potential kit (Thermo Fisher Scientific) and the IX70 Fluoview (Olympus). Cells grown on glass-bottom culture dishes (SPL) were incubated for 25 min at room temperature with the FluoVolt™ Loading Solution, which contained 1 × FluoVolt™ dye and PowerLoad™ concentrate in a physiological solution. The cells were washed three times with the physiological solution. The cells grown on glass-bottom culture dish were scanned using a standard FITC filter set on a confocal laser scanning microscope (Olympus).

Measurement of testosterone concentration

Testosterone concentration in cell supernatants was measured using a testosterone ELISA kit (Enzo Life Sciences Inc., Farmingdale, NY, USA) according to the manufacturer's instructions. TM3 cells (3×10^5 cells/well) were seeded in 6-well plates and incubated for 48 h, after which the supernatants were isolated. A steroid displacement reagent was added to the samples. Briefly, standards or samples (100 μL) were added with antibody (50 μL) to each well, mixed well, and incubated for 1 h at room temperature with shaking. Conjugates were added to each well and incubated for 1 h at room temperature with shaking. The liquid was aspirated and washed three times with 1 × wash buffer. Subsequently, pNpp substrate solution (200 μL) was added to every well and incubated for 1 h at 37℃ without shaking. Finally, stop solution (50 μL) was added to each well and tapped. The optical density of each well was read immediately using a microplate reader set to 405 nm (VERSAmax™ microplate reader; Molecular Devices, CA, USA). Testosterone concentrations were calculated from the standard curve generated throughout the experiment.

Statistical analysis

The data are presented as the mean ± S.D. A one-way ANOVA/Bonferroni test (OriginPro2020, OriginLab Corp., MA, USA) was used to assess significant differences between groups. A value of $p < 0.05$ was considered to be significant.

RESULTS

Expression pattern of c-Kit and ANO1 in testis

The H&E staining of testis revealed a normal histological appearance of seminiferous tubules. Spermatogenic cells, Sertoli cells, and Leydig cells were visible (Fig. 1A; n = 3). There was no pathological damage to the seminiferous tubules. Immunocytochemical data showed that c-Kit and ANO-1 were predominantly localized in the Leydig cells surrounding the seminiferous tubules (Fig. 1B; n = 3). c-Kit- and ANO1-positive cells showing red fluorescence were not seen in the negative control (NC) group that was not treated with the primary antibody.

Expression of c-Kit and ANO1 in Leydig cells

In the mouse testis, c-Kit and ANO1 were localized in

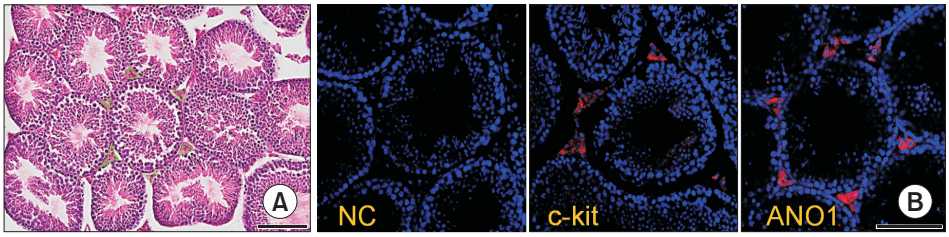

Fig. 1. Expression of c-Kit and ANO1 in Leydig cells in testis of young mice. (A) Histological image obtained by H&E staining. Leydig cells around the seminiferous tubules in the center are marked with a green line border. (B) c-Kit and ANO-1 immunostaining in testis. Red fluorescence represents c-Kit and ANO1, which are expressed in Leydig cells. Each scale bar represents 100 μm. NC, negative control.

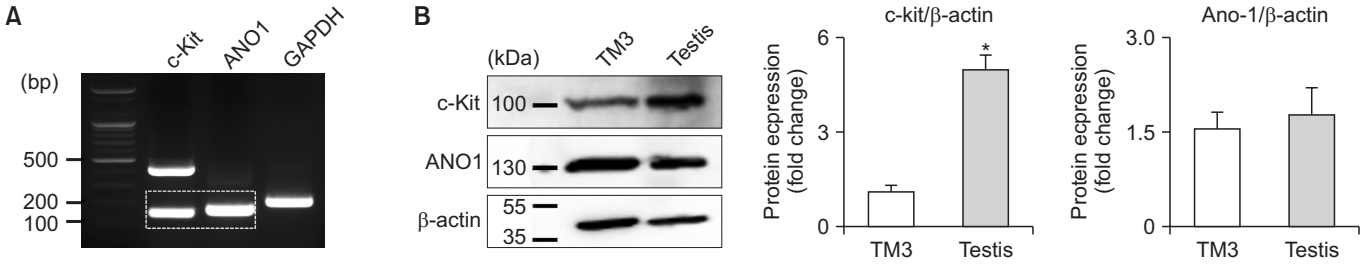

Fig. 2. Expression of c-Kit and ANO1 in TM3 Leydig cells. (A) mRNA expression of c-Kit (PCR product 150 bp) and ANO1 (PCR product 170 bp). The white dotted box indicates c-Kit and ANO1 showing the expected size. GAPDH (PCR product 201 bp) was used as a loading control. (B) Protein expression of c-Kit and ANO1. β-actin was used as a loading control. Each bar represents the mean ± SD of three independent experiments. *$p < 0.05$ compared to TM3 cells.

Leydig cells (Fig. 1). To determine the expression of c-Kit and ANO1 in Leydig cells, the TM3 mouse Leydig cell line was used. RT-PCR data showed that TM3 cells expressed c-Kit and ANO1 mRNA (Fig. 2A), and Western blotting assay revealed c-Kit and ANO1 protein expression in TM3 cells. The c-Kit expression was significantly lower in TM3 cells compared to testis tissues (Fig. 2B; n = 3, $p < 0.05$). ANO1 expression levels were similar between TM3 and testis tissues.

LH-induced increase in testosterone concentration via c-Kit and ANO1

Changes in intracellular Ca^{2+} concentration ($[Ca^{2+}]_i$), membrane potential, and testosterone concentration were analyzed in the presence of c-Kit and ANO1 inhibitors to identify if they were involved in testosterone release. Using a calcium indicator (Fluo-3 AM) and a confocal laser scanning microscope, the effect of LH on changes in $[Ca^{2+}]_i$ was examined. LH (0.1 unit/mL) elicited a rise in $[Ca^{2+}]_i$ with a Ca^{2+} oscillation wave (Fig. 3A), but pretreatment with imatinib (1 μM, a c-Kit inhibitor) significantly reduced the LH-induced increase in $[Ca^{2+}]_i$ by approximately 25% (each group n = 9, $p < 0.05$; Fig. 3A and 3B). The Ca^{2+} oscillation wave was still present in the LH + imatinib group, but the basal Ca^{2+} level was markedly lower than before chemical treatment (Fig. 3A).

FluoVolt® membrane labeling dye was used to evaluate plasma membrane potential in response to LH. LH significantly depolarized the cells, resulting in an increase in fluorescence intensity (n = 9, $p < 0.05$), whereas pretreatment with imatinib slightly decreased the fluorescence intensity (Fig. 3C).

Testosterone concentration was measured using a testosterone ELISA kit. LH induced a significant increase in testosterone secretion (Fig. 3D; $p < 0.05$, n = 4). The LH-induced secretion of testosterone was significantly reduced in the groups pretreated with imatinib and flufenamic acid (5 μM, an ANO1 inhibitor) (Fig. 3D; $p < 0.05$, n = 4).

DISCUSSION

The well-known ICC marker c-Kit is expressed in the male reproductive system, and is known to play an important role in germ cell differentiation and maturation. In adult human testis, c-Kit has been identified in the

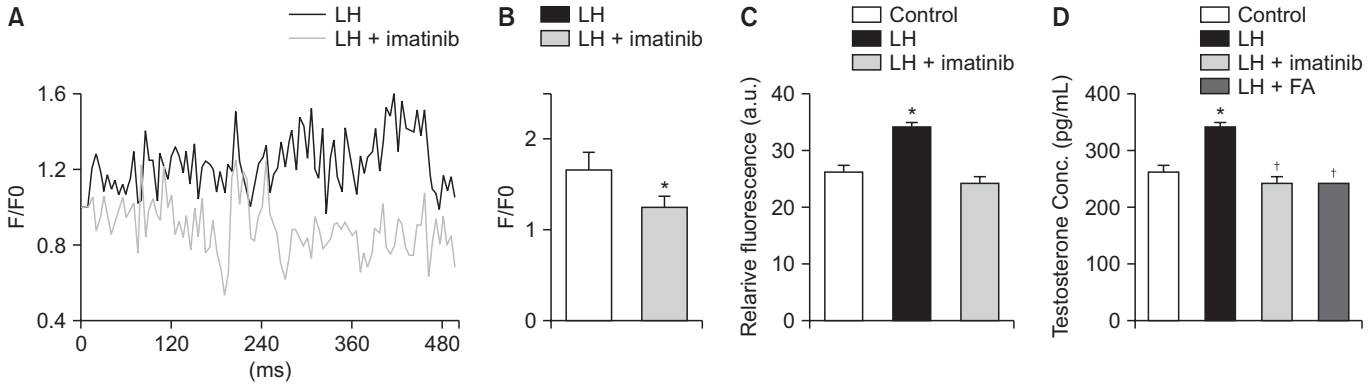

Fig. 3. Changes in $[Ca^{2+}]_i$, membrane potential, and testosterone secretion in TM3 cells induced by c-Kit and ANO1 inhibitors. (A) A representative Ca^{2+} wave in response to LH treatment. (B) Reduction in the intracellular Ca^{2+} level by c-Kit inhibition. Cells were loaded with Fluo-3 AM for 30 min, and the intensity was normalized to evaluate changes in Ca^{2+} levels. The bar graphs show the net changes in $[Ca^{2+}]_i$. *p < 0.05 compared to treatment with LH alone. Each bar represents the mean ± SD of four independent experiments. The F and F0 represent maximal fluorescence intensity and basal fluorescence intensity before treatment, respectively. (C) Changes in plasma membrane potential. Green FluoVolt® membrane labeling dye was stained and the intensity was quantified using the Fluoview software program. The bar graphs show the net changes in plasma membrane potential displayed as relative fluorescence intensity (arbitrary units, a.u.). *p < 0.05 compared to control (no treatment). (D) Testosterone concentration. After 24 h of treatment with LH in TM3 cells, the concentration of testosterone secreted from cells was measured. Each bar represents the mean ± SD of four independent experiments. *p < 0.05 compared to control. $^{\dagger}p$ < 0.05 compared to LH treatment.

membrane and cytoplasm of spermatogonia, acrosomal granules of spermatids, and Leydig cells; in particular, the level of c-Kit expression within the spermatogonia changes during spermatogenesis (Unni et al., 2009). In the present study, c-Kit was predominantly expressed in mouse Leydig cells. Expression and functional studies have demonstrated that c-Kit is identified in Leydig cells, which is associated with early maturation of spermatogenic cells (Sandlow et al., 1996; Feng et al., 1999). The Leydig cells are testosterone-producing cells in the mammalian testis, and testosterone is necessary for initiation and progression of spermatogenesis (Chung et al., 2020). The c-Kit expression in Leydig cells may be related to testosterone secretion and spermatogenesis. However, c-Kit is expressed not only in Leydig cells, but also in other cells of the male reproductive organs. c-kit-positive cells have also been identified in the space between the smooth muscle layer and the glandular layer of rat prostate (Ge et al., 2005).

The extensive expression of c-Kit led to the search for other markers that might be expressed more specifically in ICC cells. As a result, ANO1 has been suggested as another marker that could identify ICCs. In the ICCs of GI smooth muscle, ANO1 acts as a source of depolarization of smooth muscle cells, transmits slow waves, and regulates the motility of the gastrointestinal tract (Singh et al., 2014; Malysz et al., 2017; Choi et al., 2018). However, its expression in Leydig cells has not yet been explored. In the present study, we confirmed ANO1 expression in mouse Leydig cells. Leydig cells expressed both c-Kit and ANO1, which are representative ICC markers. What does the expression of these two markers mean? This seems to indicate that Leydig cells may have a function similar to ICCs.

The proposed mechanism for the generation of a rhythmic slow wave pacemaker current by ICCs in GI muscle is that the release of Ca^{2+} from the inositol 1, 4,5-trisphophate (IP_3) receptor-operated stores and activation of dihydropyridine-resistant, voltage-dependent Ca^{2+} entry. This is believed to be responsible for the initiation of slow waves, resulting in the propagation of slow waves (Ward et al., 2003; Sanders et al., 2006; Bayguinov et al., 2007; Baker et al., 2021). Slow wave generation is aided by c-Kit and ANO1. The widths of slow waves and Ca^{2+} transients are shortened by partial knockout of ANO1, while complete knockout results in the elimination of slow waves and Ca^{2+} transients, which indicates pacemaker activities (Malysz et al., 2017). ICC development is linked to c-Kit signaling (Ward et al., 1995), and the c-Kit signaling pathway is an important regulator of ICC survival and proliferation (Tong et al., 2010). ANO1 is also required for pacemaker activity (Zheng et al., 2020). In the present study, LH-induced increase in $[Ca^{2+}]_i$ was inhibited by c-Kit inhibitor treatment in mouse Leydig cell line TM3.

LH regulates testosterone synthesis in the Leydig cells by activating cholesterol desmolase (Payne and Youngblood, 1995), inducing an intracellular increase in cAMP concentration and $[Ca^{2+}]_i$ (Costa and Varanda, 2007). The calcium signaling pathway regulates Leydig cell steroidogenesis (Abdou et al., 2013). Consistent with previous studies, the present study showed that LH induced increase in $[Ca^{2+}]_i$, depolarization of membrane potential, and production of testosterone in mouse Leydig cells. c-Kit signaling is known to be associated with steroidogenesis in Leydig cells (Rothschild et al., 2003). In mice with reduced c-Kit expression, spermatogenesis is blocked after birth (Ye et al., 2017). No studies have found an association of ANO1 with steroidogenesis and spermatogenesis. LH treatment could activate c-Kit- and ANO1-associated signals, resulting in an increase in $[Ca^{2+}]_i$. The increase in $[Ca^{2+}]_i$ induced ANO1 activation and membrane depolarization.

Leydig cells isolated from testis show K^+ and Cl^- currents evoked by depolarizing voltage steps (Joffre et al., 1988), indicating that Leydig cells may have electrical properties. Submaximal testosterone production requires Ca^{2+} signaling, whereas maximal testosterone production requires Ca^{2+} and cAMP-dependent signaling (Sullivan and Cooke, 1986). Ca^{2+} signaling activated by LH induces membrane depolarization and depolarized membrane potential induces Ca^{2+} influx. Depolarization of pacemaker potential induces hormone secretion (Han et al., 2021). Enhanced Ca^{2+} signaling may be involved in the induction of testosterone secretion. In the presence of c-Kit and ANO1 inhibitors, LH-induced testosterone secretion was blocked, indicating that c-Kit and ANO1 are involved in the secretion of testosterone. Increase in $[Ca^{2+}]_i$ activates ANO1, leading to Cl^- efflux. Leydig cells are likely to act as pacemakers in testosterone secretion via c-Kit and ANO1. Further studies will be required to characterize the role of the ANO1 channel in the $[Ca^{2+}]_i$ regulation in Leydig cells. In addition, electrical characterization of primary cultured Leydig cells will be needed in future studies.

In conclusion, this study reports for the first time that ANO1 is expressed in mouse Leydig cells. In addition to c-Kit, ANO-1 can also be a marker for Leydig cells. Our results suggest that Leydig cells may act as a key driver of testicular function, particularly testosterone secretion, like ICCs, which act as pacemakers in the GI system.

Author Contributions: Conceptualization, E-A.K. and D.K.; data curation, M.S.W. and D.K.; formal analysis, M.S.W. and D.K.; funding acquisition, D.K.; investigation, M.S.W. and D.K.; methodology, M.S.W. and D.K.; project administration, M.S.W.; supervision, D.K.; validation, D.K.; visualization, M.S.W., D.K.; writing - original draft, E-A.K., D.K.; writing - review & editing, E-A.K., D.K.

Funding: This work was supported by the Basic Science Research Program through the National Research Foundation of Korea funded by the Ministry of Education (NRF-2021R1I1A3044128).

Ethical Approval: Gyeongsang National University Animal Care and Use Committee (GNU-200702-M0041).

Consent to Participate: Not applicable.

Consent to Publish: Not applicable.

Availability of Data and Materials: Not applicable.

Acknowledgements: None.

Conflicts of Interest: No potential conflict of interest relevant to this article was reported.

REFERENCES

Abdou HS, Villeneuve G, Tremblay JJ. 2013. The calcium signaling pathway regulates leydig cell steroidogenesis through a transcriptional cascade involving the nuclear receptor NR4A1 and the steroidogenic acute regulatory protein. Endocrinology 154:511-520.

Baker SA, Leigh WA, Del Valle G, De Yturriaga IF, Ward SM, Cobine CA, Drumm BT, Sanders KM. 2021. Ca^{2+} signaling driving pacemaker activity in submucosal interstitial cells of Cajal in the murine colon. Elife 10:e64099.

Bayguinov O, Ward SM, Kenyon JL, Sanders KM. 2007. Voltage-gated Ca2+ currents are necessary for slow-wave propagation in the canine gastric antrum. Am. J. Physiol. Cell Physiol. 293:C1645-C1659.

Chevalier NR, Ammouche Y, Gomis A, Teyssaire C, de Santa Barbara P, Faure S. 2020. Shifting into high gear: how interstitial cells of Cajal change the motility pattern of the developing intestine. Am. J. Physiol. Gastrointest. Liver Physiol. 319:G519-G528.

Choi S, Kang HG, Wu MJ, Jiao HY, Shin DH, Hong C, Jun JY. 2018. Effects of Ca2+-activated Cl- channel ANO1inhibitors on pacemaker activity in interstitial cells of Cajal. Cell.

Physiol. Biochem. 51:2887-2899.
Choi S, Seo H, Lee K, Shin DH, Wu MJ, Wu W, Huang X, Zhang J, Hong C, Jun JY. 2022. Hyperpolarization-activated cyclic nucleotide-gated channels working as pacemaker channels in colonic interstitial cells of Cajal. J. Cell. Mol. Med. 26:364-374.
Chung JY, Brown S, Chen H, Liu J, Papadopoulos V, Zirkin B. 2020. Effects of pharmacologically induced Leydig cell testosterone production on intratesticular testosterone and spermatogenesis†. Biol. Reprod. 102:489-498.
Costa RR and Varanda WA. 2007. Intracellular calcium changes in mice Leydig cells are dependent on calcium entry through T-type calcium channels. J. Physiol. 585(Pt 2):339-349.
Drumm BT, Hannigan KI, Lee JY, Rembetski BE, Baker SA, Koh SD, Cobine CA, Sanders KM. 2022. Ca^{2+} signalling in interstitial cells of Cajal contributes to generation and maintenance of tone in mouse and monkey lower oesophageal sphincters. J. Physiol. Advanced online publication. doi: 10.1113/JP282570
Drumm BT, Rembetski BE, Huynh K, Nizar A, Baker SA, Sanders KM. 2020. Excitatory cholinergic responses in mouse colon intramuscular interstitial cells of Cajal are due to enhanced Ca^{2+} release via M_3 receptor activation. FASEB J. 34:10073-10095.
Drumm BT, Thornbury KD, Hollywood MA, Sergeant GP. 2021. Role of Ano1 Ca^{2+}-activated Cl- channels in generating urethral tone. Am. J. Physiol. Renal Physiol. 320:F525-F536.
Edling CE and Hallberg B. 2007. c-Kit--a hematopoietic cell essential receptor tyrosine kinase. Int. J. Biochem. Cell Biol. 39:1995-1998.
Feng HL, Sandlow JI, Sparks AE, Sandra A, Zheng LJ. 1999. Decreased expression of the c-kit receptor is associated with increased apoptosis in subfertile human testes. Fertil. Steril. 71:85-89.
Ge RS, Dong Q, Sottas CM, Chen H, Zirkin BR, Hardy MP. 2005. Gene expression in rat leydig cells during development from the progenitor to adult stage: a cluster analysis. Biol. Reprod. 72:1405-1415.
Gomez-Pinilla PJ, Gibbons SJ, Bardsley MR, Lorincz A, Pozo MJ, Pasricha PJ, Van de Rijn M, West RB, Sarr MG, Kendrick ML, Cima RR, Dozois EJ, Larson DW, Ordog T, Farrugia G. 2009. Ano1 is a selective marker of interstitial cells of Cajal in the human and mouse gastrointestinal tract. Am. J. Physiol. Gastrointest. Liver Physiol. 296:G1370-G1381.
Han D, Kim JN, Kwon MJ, Han T, Kim YT, Kim BJ. 2021. *Salvia miltiorrhiza* induces depolarization of pacemaker potentials in murine small intestinal interstitial cells of Cajal via extracellular Ca^{2+} and Na^{+} influx. Mol. Med. Rep. 23:348.
Hennig GW, Spencer NJ, Jokela-Willis S, Bayguinov PO, Lee HT, Ritchie LA, Ward SM, Smith TK, Sanders KM. 2010. ICC-MY coordinate smooth muscle electrical and mechanical activity in the murine small intestine. Neurogastroenterol. Motil. 22:e138-e151.
Ishida T, Koyanagi-Aoi M, Yamamiya D, Onishi A, Sato K, Uehara K, Fujisawa M, Aoi T. 2021. Differentiation of human induced pluripotent stem cells into testosterone-producing Leydig-like cells. Endocrinology 162:bqab202.
Joffre M, Roche A, Duchatelle P. 1988. Electrophysiological studies of the action of gonadotropins on Leydig and Sertoli cells from rat testis. Reprod. Nutr. Dev. 28(4B):1019-1029.
Liu Q, Huang X, Zhang H, Tian X, He L, Yang R, Yan Y, Wang QD, Gillich A, Zhou B. 2015. c-kit(+) cells adopt vascular endothelial but not epithelial cell fates during lung maintenance and repair. Nat. Med. 21:866-868.
Loera-Valencia R, Wang XY, Wright GW, Barajas-López C, Huizinga JD. 2014. Ano1 is a better marker than c-Kit for transcript analysis of single interstitial cells of Cajal in culture. Cell. Mol. Biol. Lett. 19:601-610.
Malysz J, Gibbons SJ, Saravanaperumal SA, Du P, Eisenman ST, Cao C, Oh U, Saur D, Klein S, Ordog T, Farrugia G. 2017. Conditional genetic deletion of Ano1 in interstitial cells of Cajal impairs Ca^{2+} transients and slow waves in adult mouse small intestine. Am. J. Physiol. Gastrointest. Liver Physiol. 312:G228-G245.
Ma Y, Chen Y, Zheng Y, Wen Y, Li Y, Feng J, He Y, Wen J. 2020. SCF/c-kit signaling pathway participates in ICC damage in neurogenic bladder. Cell Cycle 19:2074-2080.
O'Donnell L, Smith LB, Rebourcet D. 2022. Sertoli cells as key drivers of testis function. Semin. Cell Dev. Biol. 121:2-9.
Parsons SP and Huizinga JD. 2020. A myogenic motor pattern in mice lacking myenteric interstitial cells of Cajal explained by a second coupled oscillator network. Am. J. Physiol. Gastrointest. Liver Physiol. 318:G225-G243.
Payne AH and Youngblood GL. 1995. Regulation of expression of steroidogenic enzymes in Leydig cells. Biol. Reprod. 52:217-225.
Popescu LM, Vidulescu C, Curici A, Caravia L, Simionescu AA, Ciontea SM, Simion S. 2006. Imatinib inhibits spontaneous rhythmic contractions of human uterus and intestine. Eur. J. Pharmacol. 546:177-181.
Rothschild G, Sottas CM, Kissel H, Agosti V, Manova K, Hardy MP, Besmer P. 2003. A role for kit receptor signaling in Leydig cell steroidogenesis. Biol. Reprod. 69:925-932.
Sanders KM. 2019. Spontaneous electrical activity and rhythmicity in gastrointestinal smooth muscles. Adv. Exp. Med. Biol. 1124:3-46.
Sanders KM, Koh SD, Ward SM. 2006. Interstitial cells of cajal as pacemakers in the gastrointestinal tract. Annu. Rev. Physiol. 68:307-343.
Sandlow JI, Feng HL, Cohen MB, Sandra A. 1996. Expression of c-KIT and its ligand, stem cell factor, in normal and subfertile human testicular tissue. J. Androl. 17:403-408.
Sferra R, Pompili S, D'Alfonso A, Sabetta G, Gaudio E, Carta G, Festuccia C, Colapietro A, Vetuschi A. 2019. Neurovascular alterations of muscularis propria in the human anterior vaginal wall in pelvic organ prolapse. J. Anat. 235:281-288.
Shafik A, Shafik I, el-Sibai O. 2005. Identification of c-kit-positive cells in the human prostate: the interstitial cells of Cajal. Arch. Androl. 51:345-351.
Singh RD, Gibbons SJ, Saravanaperumal SA, Du P, Hennig GW,

Eisenman ST, Mazzone A, Hayashi Y, Cao C, Stoltz GJ, Ordog T, Rock JR, Harfe BD, Szurszewski JH, Farrugia G. 2014. Ano1, a Ca2+-activated Cl- channel, coordinates contractility in mouse intestine by Ca2+ transient coordination between interstitial cells of Cajal. J. Physiol. 592:4051-4068.

Siregar AS, Nyiramana MM, Kim EJ, Shin EJ, Kim CW, Lee DK, Hong SG, Han J, Kang D. 2019. TRPV1 is associated with testicular apoptosis in mice. J. Anim. Reprod. Biotechnol. 34:311-317.

Sullivan MH and Cooke BA. 1986. The role of Ca2+ in steroidogenesis in Leydig cells. Stimulation of intracellular free Ca2+ by lutropin (LH), luliberin (LHRH) agonist and cyclic AMP. Biochem. J. 236:45-51.

Tamada H and Kiyama H. 2015. Existence of c-Kit negative cells with ultrastructural features of interstitial cells of Cajal in the subserosal layer of the W/W(v) mutant mouse colon. J. Smooth Muscle Res. 51:1-9.

Tong W, Jia H, Zhang L, Li C, Ridolfi TJ, Liu B. 2010. Exogenous stem cell factor improves interstitial cells of Cajal restoration after blockade of c-kit signaling pathway. Scand. J. Gastroenterol. 45:844-851.

Unni SK, Modi DN, Pathak SG, Dhabalia JV, Bhartiya D. 2009. Stage-specific localization and expression of c-kit in the adult human testis. J. Histochem. Cytochem. 57:861-869.

Wang JP, Ding GF, Wang QZ. 2013. Interstitial cells of Cajal mediate excitatory sympathetic neurotransmission in guinea pig prostate. Cell Tissue Res. 352:479-486.

Ward SM, Baker SA, de Faoite A, Sanders KM. 2003. Propagation of slow waves requires IP3 receptors and mitochondrial Ca2+ uptake in canine colonic muscles. J. Physiol. 549(Pt 1):207-218.

Ward SM, Burns AJ, Torihashi S, Harney SC, Sanders KM. 1995. Impaired development of interstitial cells and intestinal electrical rhythmicity in steel mutants. Am. J. Physiol. 269(6 Pt 1):C1577-C1585.

Wishahi M, Hafiz E, Wishahy AMK, Badawy M. 2021. Telocytes, c-Kit positive cells, Smooth muscles, and collagen in the ureter of pediatric patients with congenital primary obstructive megaureter: elucidation of etiopathology. Ultrastruct. Pathol. 45:257-265.

Yang JH, Siregar AS, Kim EJ, Nyiramana MM, Shin EJ, Han J, Sohn JT, Kim JW, Kang D. 2019. Involvement of TREK-1 channel in cell viability of H9c2 rat cardiomyoblasts affected by bupivacaine and lipid emulsion. Cells 8:454.

Ye L, Li X, Li L, Chen H, Ge RS. 2017. Insights into the development of the adult Leydig cell lineage from stem Leydig cells. Front. Physiol. 8:430.

Zheng H, Drumm BT, Zhu MH, Xie Y, O'Driscoll KE, Baker SA, Perrino BA, Koh SD, Sanders KM. 2020. Na^+/Ca^{2+} exchange and pacemaker activity of interstitial cells of Cajal. Front. Physiol. 11:230. (Erratum published 2020, Front. Physiol. 11:362)

Zirkin BR and Papadopoulos V. 2018. Leydig cells: formation, function, and regulation. Biol. Reprod. 99:101-111.